Ms. for *Journal of Molecular Structure* (INVITED ARTICLE FOR THE SPECIAL ISSUE ENTITLED "CHARGE-DENSITY STUDIES TOWARDS STRUCTURE-PROPERTY CORRELATION")

# Two octahedral σ-borane metal ($Mn^{I}$ and $Ru^{II}$) complexes containing a tripod $\kappa^3$*N,H,H*-ligand: Synthesis, structural characterization, and theoretical topological study of the charge density

Juan F. Van der Maelen[a,b,*], Javier Brugos[c], Pablo García-Álvarez[c], Javier A. Cabeza[c]

[a]*Departamento de Química Física y Analítica, Universidad de Oviedo, E-33006 Oviedo, Spain*

[b]*Centro de Investigación en Nanomateriales y Nanotecnología (CINN-CSIC), E-33940 El Entrego, Spain*

[c]*Departamento de Química Orgánica e Inorgánica and Centro de Innovación en Química Avanzada (ORFEO-CINQA), Universidad de Oviedo, E-33006 Oviedo, Spain*

*Corresponding author.

*E-mail address:* fvu@uniovi.es (J. F. Van der Maelen)

**Abstract**

Theoretical electron density (QTAIM) studies in the gas-phase have shown that the attachment of the $BH_3$ group to the metal atom in complexes [Mn($\kappa^3$*N,H,H*-$^i$Pr$_2$bzamBH$_3$)(CO)$_3$] **(1)** and [Ru($\eta^5$-$C_5Me_5$)($\kappa^3$*N,H,H*-$^i$Pr$_2$bzamBH$_3$)] **(2)** ($H^iPr_2$bzamBH$_3$ = N-trihydridoborane-N,N'-bis(isopropyl) benzamidine) is symmetric in the latter but asymmetric in the former, and involves two B–H–metal interactions that are intermediate between $\kappa^1$*H* (Shimoi type) and $\kappa^2$*H,B* (agostic type). The herein reported results, coupled to previous ones on related complexes having a similar tripod $\kappa^3$*N,H,H*-borane ligand, show that the bonding similarities and differences within each particular M($\mu$-H)$_2$B moiety are not related to the type of metal atom, nor even to its coordination geometry, but mainly to the molecular symmetry.

**Keywords:** Quantum Theory of Atoms in Molecules (QTAIM), Electron Localization Function (ELF), σ-Borane Complexes, Transition-Metal Carbonyl Complexes, Multicenter Bonding, Chemical Bonding.

## 1. Introduction

In the last two decades, the analysis of the electron density's topology under the perspective of the Quantum Theory of Atoms in Molecules (QTAIM) [1] has been established as a powerful tool, complementary to the Molecular Orbital (MO) theory, to analyze chemical bonds. QTAIM studies on systems containing light atoms (periods 1–3 of the periodic table) have allowed the establishment of useful links between bonding modes and topological properties of the electron density (both local and integral) and its Laplacian, from both theoretically- and experimentally-determined electron densities [2]. However, such links cannot be straightforwardly extended to compounds with transition-metal atoms since the latter display a different and much narrower spectrum of topological indexes [3]. For this reason, there is a general consensus among experts in the field about the urgent need for more work in this area, in order to derive accurate correspondence rules that could unambiguously be applicable to any kind of bonding interactions involving one or more transition-metal atoms, particularly when regarding multiple bond orders and/or multicenter bonding [4].

The increasing interest in the use of amine−boranes ($H_2RNBH_2R'$; R, R′ = H, alkyl, aryl) as molecular systems for hydrogen storage and transportation [5] and the discovery that transition-metal complexes can promote their dehydrogenation to give $H_2$ (or the transfer of $H_2$ to other molecules) [6,7] have recently boosted the study of their coordination chemistry [8,9], as well as that of aminoboranes (HRNBHR′; R, R′ = H, alkyl, aryl) [10], which are intermediates in the dehydrogenation of amine−boranes. In all these complexes, the ligand is attached to the metal atom almost exclusively through one or two of the BH groups (σ-complexes) [11], involving either $\kappa^2$*H,B* (agostic interaction: both atoms of the BH group interact with the metal) or $\kappa^1$*H* (Shimoi interaction: only the H atom of the BH group is attached to the metal) interactions. In any of the two cases, borane−metal interactions are usually weak [12].

In this context, we have recently described [13] the synthesis, experimental structural characterization and QTAIM studies of the octahedral complexes [Mn($\kappa^3$*N,H,H*-mapyBH$_3$)(CO)$_3$] **(3)** and [RuH($\kappa^3$*N,H,H*-mapyBH$_3$)(CO)(P$^i$Pr$_3$)] **(4)**, and the pentacoordinated complexes [M($\kappa^3$*N,H,H*-mapyBH$_3$)($\eta^4$-cod)] (M = Rh **(5)**, Ir **(6)**; HmapyBH$_3$ = N-trihydridoborane-2-(methylamino)pyridine; cod = cycloocta-1,5-diene). In the four cases we found that: (a) all M–H interactions with the $BH_2$ group show bond paths that are strongly inwardly curved, with greater deviations from a straight line near the hydrogen atoms than near the metal centers; (b) no M–B bond paths were obtained, although non-negligible values were always calculated for the delocalization indexes of these interactions; (c) all

M–HB bonds are intermediate between those of the Shimoi type ($\kappa^1H$ coordination) and those of the agostic type ($\kappa^2H,B$ coordination). On the other hand, while both M–HB bonds were found to be equivalent for the Mn compound, they are not equivalent for the Ru, Rh, and Ir complexes, with one bond more agostic (more curved, higher ellipticity) than the other (less curved, lower ellipticity).

In order to further explore the influence of the metal complex symmetry and that of the ligands themselves in the bonding of this important class of borane derivatives, we decided to study two additional complexes, that is, [Mn($\kappa^3N,H,H$-$^i$Pr$_2$bzamBH$_3$)(CO)$_3$] (**1**) and [Ru($\eta^5$-C$_5$Me$_5$)($\kappa^3N,H,H$-$^i$Pr$_2$bzamBH$_3$)] (**2**) (H$^i$Pr$_2$bzamBH$_3$ = N-trihydridoborane-N,N'-bis(isopropyl)benzamidine) (Scheme 1), which were selected not only because their ligands differ from those of the four complexes previously reported (**3-6**) but also because they include the same metal atoms as two of them (Mn, Ru) and have an *a priori* identical coordination geometry (octahedral). As a consequence, bonding comparisons between **1** and **2** with the previously studied complexes could be made more straightforwardly and mostly centered on the nature of the ligands. We report here the synthesis and structural characterization of the borane adduct H$^i$Pr$_2$bzamBH$_3$ and its metal derivatives **1** and **2**, as well as a theoretical topological analysis of the bonding in the three compounds.

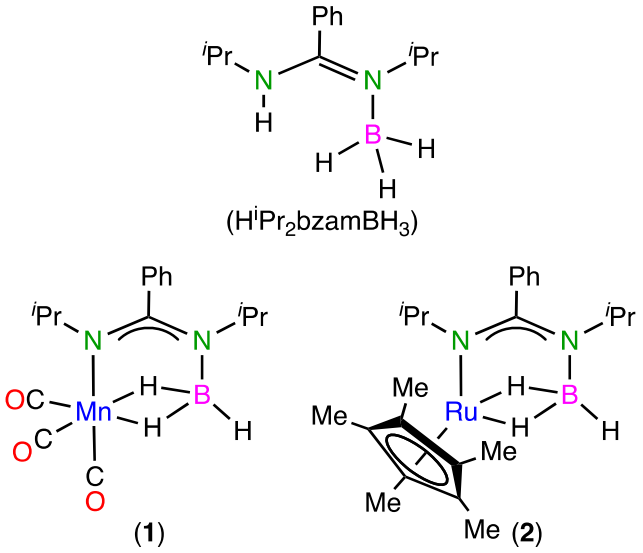


**Scheme 1.** Molecular diagrams of H$^i$Pr$_2$bzamBH$_3$, **1** and **2**

## 2. Experimental and computational details

## 2.1. Synthetic procedures and spectroscopic data

**General experimental data:** Solvents were dried over appropriate desiccating reagents and were distilled under argon before use. All reactions and manipulations were carried out under argon, using dry box and/or Schlenk-vacuum line techniques. All reaction products were vacuum-dried for several hours prior to being weighed and analysed. The metal complex $[Ru_2(\eta^5\text{-}C_5Me_5)_2Cl_4]$ was prepared following a published procedure [14]. All remaining reagents were purchased from commercial suppliers. NMR spectra were obtained on Bruker DPX-300, NAV-400 and AV400 instruments and were referenced using the residual protic solvent signal for $^1$H (7.16 ppm for d$^6$-benzene), the solvent signal for $^{13}$C (128.1 ppm for d$^6$-benzene) and external $F_3B{\cdot}OEt_2$ for $^{11}$B [$\delta$ = 0.00 ppm].

**H$^i$Pr$_2$bzamBH$_3$:** PhLi (1.1 mL, 2.0 mmol, 1.8 M in dibutyl ether) was added dropwise to a solution of *N*,*N'*-bis(isopropyl)carbodiimide (0.3 mL, 2.0 mmol) in diethyl ether (3 mL) at 78º C. The resulting white suspension was allowed to warm up to room temperature and then stirred for 3 h. Deoxygenated water (0.08 mL, 4.4 mmol) was added to the previous suspension, which was then stirred for 30 min. The solvent was removed under reduced pressure and the resulting whitish oily residue was extracted into dichloromethane (2 x 5 mL), drying the resulting solution with $Na_2SO_4$, which was then filtered with a cannula fitted with a small piece of filter paper wrapped around one of its ends. Solvent removal under reduced pressure of the filtrate led to a yellowish oil, which was identified as *N*,*N'*-bis(isopropyl)benzamidine (H$^i$Pr$_2$bzam) by $^1$H-NMR analysis. The previous oil was dissolved in 2 mL of toluene and subsequently was added dropwise to a solution of $BH_3{\cdot}THF$ (2.4 mL, 2.4 mmol, 1.0 M in THF) at 78º C. The resulting colourless solution was stirred at 78º C for 1h. Solvent removal allowed the isolation of H$^i$Pr$_2$bzamBH$_3$ as a white solid that was washed with hexane (2 x 3 mL) and dried in vacuo (314 mg, 72%). $^1$H NMR ($C_6D_6$, 400.54 MHz, 298 K): $\delta$ 7.10-6.90 (m, 3 H, 3 C*H* of Ph), 6.90-6.80 (m, 2 H, 2 C*H* of Ph), 3.42 (sept, $J_{H-H}$ = 6.0 Hz, 1 H, 1 C*H* of $^i$Pr), 2.76 (m, 1 H, 1 C*H* of $^i$Pr), 2.64 (br q, $J_{H-11B}$ = 85.9 Hz, 3 H, B*H*$_3$), 1.31 (d, $J_{H-H}$ = 6.0 Hz, 6 H, 2 C*H*$_3$ of $^i$Pr), 0.70 (d, $J_{H-H}$ = 6.0 Hz, 6 H, 2 C*H*$_3$ of $^i$Pr). $^{11}$B NMR ($C_6D_6$, 128.51 MHz, 298 K): $\delta$ –23.6 (br q, $J_{H-11B}$ = 85.9 Hz, *B*H$_3$), this signal collapses to a singlet in a $^{11}$B{$^1$H} NMR spectrum. $^{13}$C{$^1$H} NMR ($C_6D_6$, 75.5 MHz, 293 K): $\delta$ = 160.9 (N*C*N), 131.8 (*C*$_{ipso}$ of Ph), 130.0 (*C*H of Ph), 129.3 (2 *C*H of Ph), 127.1 (2 *C*H of Ph), 52.6 (1 *C*H of $^i$Pr), 46.1 (1 *C*H of $^i$Pr), 24.0 (2 *C*H$_3$ of $^i$Pr), 21.8 (2 *C*H$_3$ of $^i$Pr).

**[Mn($\kappa^3$*N*,*H*,*H*-$^i$Pr$_2$bzamBH$_3$)(CO)$_3$] (1):** LiN(SiMe$_3$)$_2$ (0.1 mL, 0.1 mmol, 1 M in hexane) was added dropwise to a solution of H$^i$Pr$_2$bzamBH$_3$ (22 mg, 0.1 mmol) in toluene (3 mL) at room temperature. The resulting yellowish solution was then stirred for 1 h, which allowed the formation of the lithiated

salt Li$^{i}$Pr$_2$bzamBH$_3$. Then, this solution was added dropwise at room temperature to a yellow solution of [MnBr(CO)$_3$(NCMe)$_2$] (0.1 mmol) in CH$_3$CN (8 mL), which was previously prepared by refluxing [MnBr(CO)$_5$] (28 mg, 0.1 mmol) in CH$_3$CN (8 mL) for 15 min. The resulting yellowish solution was then stirred for 30 min. IR (ν(CO) analysis indicated no reaction completion. The solvents were removed under reduced pressure and the resulting yellowish residue was dissolved in toluene (5 mL) and the resulting solution was stirred at 50 ºC for 1 h. The colour changed from yellow to orange. An IR analysis (ν(CO) region) indicated the consumption of all the starting materials. Complex **1**, isolated as an orange solid (14 mg, 40%), was purified by column chromatography in silica gel, using hexane as eluant. IR (toluene): $\nu_{CO}$ 2031 (s), 1937 (vs, br) cm$^{-1}$. $^1$H{$^{11}$B} NMR (C$_6$D$_6$, 400.54 MHz, 298 K): δ 6.97 (br, 3 H, 3 C*H* of Ph), 6.62 (br, 2 H, 2 C*H* of Ph), 4.83 (s, br, 1 H, *H*BH$_2$), 386 (s, br, 1 H, 1 C*H* of $^{i}$Pr), 3.23 (s, br, 1 H, 1 C*H* of $^{i}$Pr), 1.23 (s, 6 H, 2 C*H*$_3$ of $^{i}$Pr), 0.94 (s, 6 H, 2 C*H*$_3$ of $^{i}$Pr), –9.88 (s, br, 2 H, Mn*H*$_2$B); the broad singlets at 4.83 and −9.88 ppm are transformed into two broad multiplets in a $^1$H NMR spectrum. $^{11}$B{$^1$H} NMR (C$_6$D$_6$, 128.51 MHz, 298 K): δ –19.6 (s, br, *B*H$_3$), this signal becomes broader in a $^{11}$B NMR spectrum. $^{13}$C{$^1$H} NMR (C$_6$D$_6$, 100.6 MHz, 293 K): δ = 171.4 (N*C*N), 136.1 (*C*$_{ipso}$ of Ph), 129.1–127.0 (5 *C*Hs of Ph), 56.4 (1 *C*H of $^{i}$Pr), 50.7 (1 *C*H of $^{i}$Pr), 26.3 (2 *C*H$_3$ of $^{i}$Pr), 23.6 (2 *C*H$_3$ of $^{i}$Pr). The resonances corresponding to the carbonyl ligands were not observed.

**[Ru(η$^5$-C$_5$Me$_5$)(κ$^3$*N*,*H*,*H*-$^{i}$Pr$_2$bzamBH$_3$)] (2):** LiN(SiMe$_3$)$_2$ (0.1 mL, 0.1 mmol, 1 M in hexane) was added dropwise to a solution of H$^{i}$Pr$_2$bzamBH$_3$ (18 mg, 0.08 mmol) in toluene (5 mL) at room temperature. The resulting yellowish solution was then stirred for 1 h, which allowed the formation of Li$^{i}$Pr$_2$bzamBH$_3$. Then, this solution was added dropwise at room temperature to [Ru$_2$(η$^5$-C$_5$Me$_5$)$_2$Cl$_4$] (25 mg, 0.04 mmol). The resulting brownish orange suspension was then stirred overnight and was then filtered with a cannula fitted with a small piece of filter paper wrapped around one of its ends. The solvents of the filtrate (red solution) were removed under reduced pressure and the resulting dark brown residue was extracted into hexane (3 mL). Solvent removal allowed the isolation of **3** as a dark orange solid that was dried in vacuo (18 mg, 41%). $^1$H NMR (C$_6$D$_6$, 400.54 MHz, 298 K): δ 7.05-6.90 (m, 3 H, 3 C*H* of Ph), 6.90-6.85 (m, 2 H, 2 C*H* of Ph), 4.81 (br q, $J_{H-11B}$ = 113.3 Hz, 2 H, HB*H*$_2$), 3.81 (s, br, 1 H, 1 C*H* of $^{i}$Pr), 3.40 (m, 1 H, 1 C*H* of $^{i}$Pr), 1.95 (s, 15 H, 5 C*H*$_3$ of C$_5$Me$_5$), 1.45 (s, br, 6 H, 2 C*H*$_3$ of $^{i}$Pr), 1.20 (d, $J_{H-H}$ = 8.0 Hz, 6 H, 2 C*H*$_3$ of $^{i}$Pr), –9.11 (m, br, 2 H, Ru*H*$_2$B); the broad signals at 4.81 and −9.11 ppm collapse to singlets in a $^1$H{$^{11}$B} NMR spectrum. $^{11}$B NMR (C$_6$D$_6$, 128.51 MHz, 298 K): δ –16.4 (s, br, *B*H$_3$), this signal does not change in a $^{11}$B{$^1$H} NMR spectrum.

### 2.2. X-Ray diffraction analyses

Crystals of $H^iPr_2bzamBH_3 \cdot 0.5(C_7H_8)$ (obtained by slow evaporation of a solution of the borane adduct in toluene), **1** (obtained by slow evaporation of a solution of the complex in toluene) and **2** (obtained by keeping at –20 ºC for 12 h a concentrated solution of the complex in toluene) were analysed by X-ray diffraction. A selection of crystal, measurement and refinement data is given in Table S1 of the Supplementary Material. Diffraction data were collected at 150(2) K on an Oxford Diffraction Xcalibur Onyx Nova single crystal diffractometer. Empirical absorption corrections were applied using the SCALE3 ABSPACK algorithm as implemented in CrysAlisPro RED [15]. The structures were solved using SIR-97 [16]. Isotropic and full matrix anisotropic least square refinements were carried out using SHELXL-2014 [17]. All non-H atoms were refined anisotropically. Hydrogen atoms of the $BH_3$ moieties were located in their corresponding Fourier maps. The remaining hydrogen atoms were set in calculated positions and refined riding on their parent atoms. The toluene molecules found in the crystal of $H^iPr_2bzamBH_3 \cdot 0.5(C_7H_8)$ were disordered about centres of symmetry and required restraints on their geometrical and thermal parameters. The WINGX-2013 program system [18] was used throughout structure determinations. Molecular plots were made with MERCURY [19]. CCDC deposition numbers: 1921463 ($H^iPr_2bzamBH_3 \cdot 0.5(C_7H_8)$), 1921464 (**1**), and 1921465 (**2**).

### 2.3. DFT calculations and theoretical charge density studies

It has been previously shown that the use of relativistic hamiltonians is essential in order to obtain accurate quantitative results from calculations on compounds containing third-row transition-metal atoms [20], but the effect of using such hamiltonians on calculations involving second-row transition metals is not yet clear. In order to compare our new results with the previously published ones [13], we have used here exactly the same model chemistries (Hamiltonians, funcionals, and basis sets) than before.

The X-ray diffraction (XRD) molecular structures of complexes **1** and **2** were used as starting points to calculate the theoretically optimized geometries in gas phase. Density Functional Theory (DFT) computations with non-relativistic wavefunctions were performed with the GAUSSIAN09 program package [21], using the B3P86 hybrid functional, which is known to give accurate results in medium-sized transition-metal organometallic compounds [22]. All-electron 6-31G(d,p) and 6-311++G(2df,2pd) standard basis sets were employed for Mn, C, H, N, and O atoms at different steps of the procedure (the former basis set for the geometry optimizations and the latter for the single-point

electronic structure calculations at the optimized geometries), while the LanL2DZ effective core potential and the large all-electron WTBS basis set ("Well-Tempered Basis Set" of Huzinaga and co-workers [23]) were used for Ru atoms (again, the former for the geometry optimizations and the latter for the electronic structure calculations).

Computations with relativistic wavefunctions were performed using the scalar ZORA hamiltonian, the PW91 density functional, and the all-electron relativistic QZ4P basis set for all atoms [24], as implemented in the ADF2012 program package [25], in order to obtain relativistically optimized geometries, while the hybrid ZORA-B1PW91 model with relativistic QZ4P basis sets were then used for single-point electronic structure calculations at the optimized geometries.

The obtained non-relativistic and relativistic ground-state electronic wavefunctions, which were found to be stable, were then utilized for calculations on the topology of the electron density within the framework of the QTAIM approach. These calculations included both local and integral properties and were carried out with AIMAll [26], AIM2000 [27], and DGrid [28] programs from GTO- and STO-based wavefunctions. The accuracy of local properties was $1.0\times10^{-10}$ (from the gradient of the electron density at the bond critical points), whereas that of integral properties was finally set at least at $1.0\times10^{-4}$ (from the Laplacian of the integrated electron density). Both all-electron non-relativistic B3P86/6-311++G(2df,2pd)/WTBS(Ru) and relativistic ZORA-B1PW91/QZ4P models, applied to the theoretically optimized geometries, were used in all cases to find critical points and calculate topological parameters.

## 3. Results and discussion

The previously unknown borane adduct H$^{i}$Pr$_2$bzamBH$_3$ was straightforwardly prepared by treating *N*,*N'*-bis(isopropyl)benzamidine (H$^{i}$Pr$_2$bzam) with BH$_3$·THF. Complexes **1** and **2** were synthesized by reacting [MnBr(CO)$_3$(NCMe)$_2$] and [Ru$_2$($\eta^5$-C$_5$Me$_5$)$_2$Cl$_4$] with Li$^{i}$Pr$_2$bzamBH$_3$. The latter was formed *in situ* by treating H$^{i}$Pr$_2$bzamBH$_3$ with LiN(SiMe$_3$)$_2$ prior to its reaction with the corresponding metal complex (see the previous "Experimental and computational details" section for synthetic details and spectroscopic data). As may be seen in Figure 1, XRD analyses performed at 150(2) K confirm the tripod $\kappa^3$*N,H,H* coordination of the $^{i}$Pr$_2$bzamBH$_3$ ligand in **1** and **2**, as well as the octahedral environment of both Mn and Ru atoms (in **2**, the C$_5$Me$_5$ ligand occupies three coordination sites).

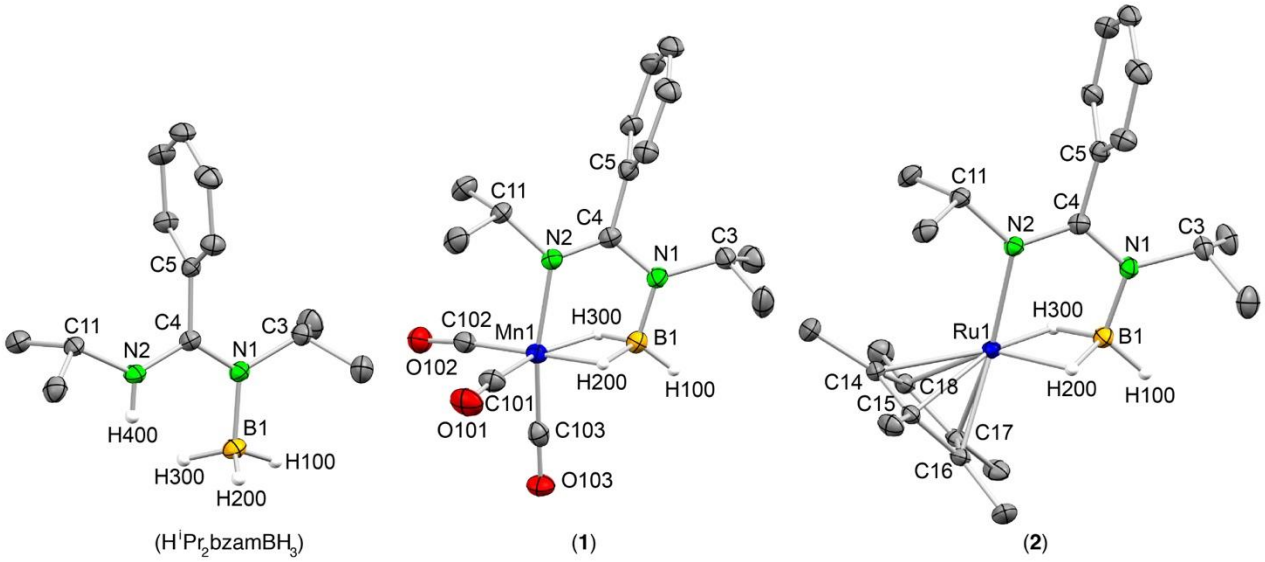


**Fig. 1** XRD molecular structures of H$^{i}$Pr$_2$bzamBH$_3$, **1** and **2** (ellipsoids drawn at 30% probability). Hydrogen atoms of methyl, isopropyl and phenyl groups are omitted for clarity.

A close inspection of the experimental (XRD) metric data concerning the Mn atom and the atoms of the $BH_3$ group of complex **1** (Table 1) reveals that those involving H200 (Mn1–H200 1.49(6) Å, B1–H200 1.34(6) Å, Mn1–H200–B1 98(3)°) exhibit significant differences from those involving H300 (Mn1–H300 1.59(6) Å, B1–H300 1.13(6) Å, Mn1–H300–B1 102(4)°). Regarding complex **2** (Table 2), the data involving H200 (Ru1–H200 1.71(3) Å, B1–H200 1.29(3) Å, Ru1–H200–B1 92(1)°) are almost identical to those involving H300 (Ru1–H300 1.72(3) Å, B1–H300 1.32(2) Å, Ru1–H300–B1 90(1)°). As the XRD data involving the H200 and H300 atoms of **1** and **2** might be affected by packing effects in the solid state as well as by experimental errors (some differences are within the estimated standard deviations and it is well known that XRD is not the best method to locate hydrogen atoms accurately), we decided to theoretically optimize the gas phase molecular structures of **1** and **2** without symmetry restraints. The obtained results (Tables 1 and 2) show that only the relativistic method rendered a perfectly symmetric $C_S$ structure for complex **2**, while for **1** both methods (relativistic and non-relativistic) deviate slightly from this symmetry, giving structures where, rather surprisingly, the two N$^{i}$Pr ligands are not arranged in a fully eclipsed manner but twisted (tables of theoretical coordinates are provided in the Supplementary Material).

**Table 1**
Experimental (XRD) and theoretical (DFT) interatomic distances (Å) and angles (°) in complex **1**.

| *Atoms* | *Experimental (XRD)* | *ZORA-PW91/QZ4P* | *B3P86/ 6-31G(d,p)* |
|---|---|---|---|

| | | | |
|---|---|---|---|
| Mn1–B1 | 2.132(5) | 2.128 | 2.115 |
| Mn1–H200 | 1.49(6) | 1.678 | 1.673 |
| Mn1–H300 | 1.59(6) | 1.703 | 1.698 |
| Mn1–N2 | 2.071(3) | 2.065 | 2.047 |
| Mn1–C101 | 1.825(5) | 1.784 | 1.780 |
| Mn1–C102 | 1.817(5) | 1.791 | 1.782 |
| Mn1–C103 | 1.801(5) | 1.787 | 1.782 |
| B1–H100 | 1.08(6) | 1.195 | 1.195 |
| B1–H200 | 1.34(6) | 1.321 | 1.312 |
| B1–H300 | 1.13(6) | 1.315 | 1.308 |
| H200–Mn1–H300 | 70(3) | 75.7 | 75.6 |
| Mn1–H200–B1 | 98(3) | 89.6 | 89.4 |
| Mn1–H300–B1 | 102(4) | 88.7 | 88.5 |
| H200–B1–H300 | 90(4) | 103.8 | 104.1 |
| N1–C4–N2 | 118.5(3) | 118.1 | 118.5 |

**Table 2**
Experimental (XRD) and theoretical (DFT) interatomic distances (Å) and angles (°) in complex **2**.

| *Atoms* | *Experimental (XRD)* | *ZORA-PW91/QZ4P* | *B3P86/ 6-31G(d,p)/ LanL2DZ(Ru)* |
|---|---|---|---|
| Ru1–B1 | 2.173(3) | 2.169 | 2.177 |
| Ru1–H200 | 1.71(3) | 1.749 | 1.757 |
| Ru1–H300 | 1.72(3) | 1.749 | 1.761 |
| Ru1–N2 | 2.133(2) | 2.141 | 2.139 |
| Ru1–C14 | 2.250(2) | 2.284 | 2.291 |
| Ru1–C15 | 2.198(2) | 2.211 | 2.222 |
| Ru1–C16 | 2.143(2) | 2.152 | 2.164 |
| Ru1–C17 | 2.147(2) | 2.152 | 2.167 |
| Ru1–C18 | 2.189(2) | 2.210 | 2.217 |
| B1–H100 | 1.13(3) | 1.203 | 1.199 |
| B1–H200 | 1.29(3) | 1.343 | 1.335 |
| B1–H300 | 1.32(2) | 1.344 | 1.333 |
| H200–Ru1–H300 | 73(1) | 75.9 | 74.8 |
| Ru1–H200–B1 | 92(1) | 88.0 | 88.4 |
| Ru1–H300–B1 | 90(1) | 88.0 | 88.3 |
| H200–B1–H300 | 103(2) | 106.4 | 106.4 |
| N1–C4–N2 | 118.3(2) | 118.1 | 118.7 |

**Table 3**
Experimental (XRD) and theoretical (DFT) interatomic distances (Å) and angles (°) in the borane adduct $H^iPr_2bzamBH_3$.

| *Atoms* | *Experimental (XRD)* | *ZORA-PW91/QZ4P* | *B3P86/ 6-31G(d,p)* |
|---|---|---|---|
| B1–H100 | 1.13(2) | 1.207 | 1.207 |
| B1–H200 | 1.13(2) | 1.229 | 1.223 |

| | | | |
|---|---|---|---|
| B1–H300 | 1.13(2) | 1.225 | 1.223 |
| H100–B1–H200 | 112(1) | 110.2 | 111.1 |
| H100–B1–H300 | 110(1) | 111.0 | 111.1 |
| H200–B1–H300 | 108(1) | 109.5 | 110.2 |
| N1–C4–N2 | 120.3(1) | 117.7 | 118.7 |

The images depicted in Figure 2 were obtained by applying the QTAIM approach to the theoretically optimized geometries of compounds **1** and **2**. They show, along with the atoms corresponding to each complex, the complete set of bond critical points (*bcp*'s), ring critical points (*rcp*'s), and a cage critical point (*ccp*), together with bond paths (*bp*'s) connecting bonded atoms through their corresponding *bcp*'s. As clearly seen in Figure 2, no *bp* has been found between metal and boron atoms in any of the two complexes, while M–H200 and M–H300 *bp*'s, as well as H200–B1 and H300–B1 *bp*'s, were found in each compound. Additionally, a *rcp*, located inside each M(μ-H)$_2$B ring, was obtained for each complex.

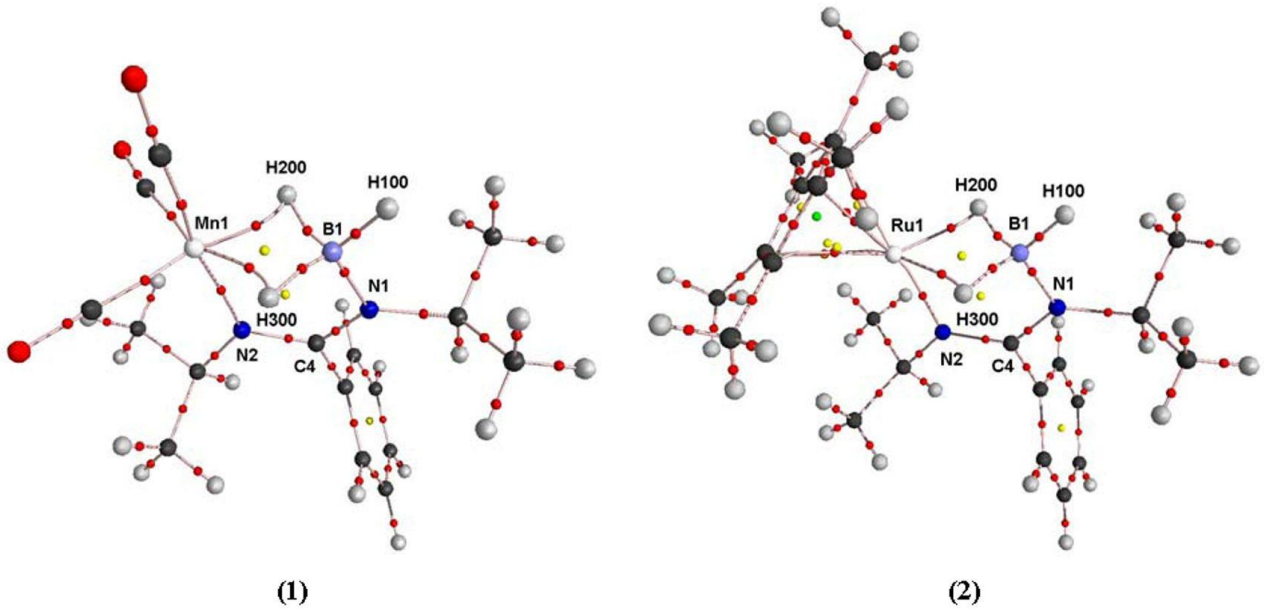


**Fig. 2** Topological graphs (B3P86/6-311++G(2df,2pd)/WTBS(Ru) level) of compounds **1** and **2**, showing bond paths (solid lines) and bond (small red circles), ring (small yellow circles) and cage (small green circle) critical points. The graph of the borane adduct H$^i$Pr$_2$bzamBH$_3$ is shown in the Supplementary Material.

A closer view of the M(μ-H)$_2$B ring is depicted in Figure 3, where the gradient trajectory map of the total electron density in the H200–M–H300 plane of both complexes is displayed, showing *bp*'s and basins of the atoms contained in the chosen plane. As clearly seen in Figure 3, no M–H *bp* is a straight line, being strongly inwardly curved, with approximately the same curvature for the Ru1–H200 and Ru1–H300 interactions, but slightly different for the Mn1–H200 and Mn1–H300 interactions. As a

consequence, the *rcp* for complex **2** is symmetrically located at the gravity center of the Ru1(μ-H)$_2$B1 ring, while for **1** it is slightly displaced towards the Mn1–H300 *bcp*. Therefore, it is suggested that the Ru1–H200 and Ru1–H300 interactions are equivalent to each other, as well as the B1–H200 and B1–H300 interactions in **2**, while for complex **1** they are not completely equivalent (see forthcoming tables for a more quantitative comparison).

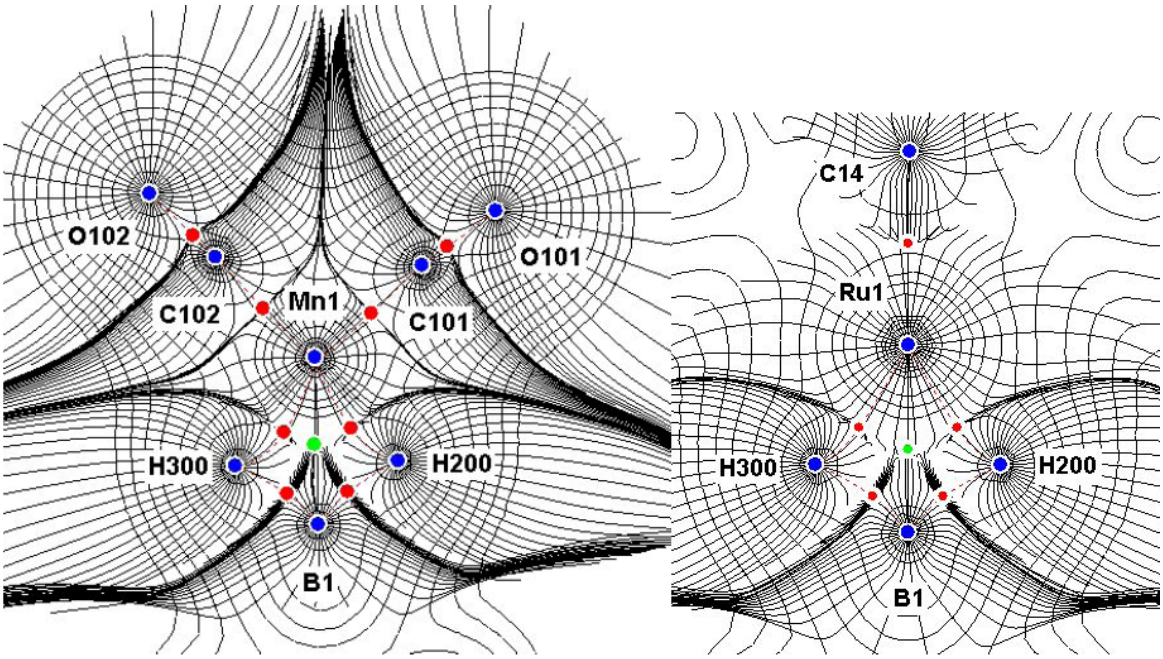


**Fig. 3** Gradient trajectories (B3P86/6-311++G(2df,2pd)/WTBS(Ru) level) mapped on total electron density plots (contour levels at 0.1 e Å$^{-3}$) in H200–M–H300 planes containing the metal atoms of compounds **1** and **2**, showing the atomic basins, *bp*'s (dashed red lines), *bcp*'s (red circles), and a *rcp* (green circle). Larger images are included in the Supplementary Material file.

Integration of the electron density inside each atomic basin rendered the electric charge, *Q*, of each atom. Table 4 compares relativistic QTAIM charges of selected atoms of **1** and **2** among them and also with those previously published for the above mentioned complexes [Mn(κ$^3$*N,H,H*-mapyBH$_3$)(CO)$_3$] (**3**), [RuH(κ$^3$*N,H,H*-mapyBH$_3$)(CO)(P$^i$Pr$_3$)] (**4**), [Rh(κ$^3$*N,H,H*-mapyBH$_3$)(η$^4$-cod)] (**5**), and [Ir(κ$^3$*N,H,H*-mapyBH$_3$)(η$^4$-cod)] (**6**) [13]. Rather interestingly, the atomic charge of the Mn atom in **1** and **3** coincides with its formal charge (+1), while that of the corresponding M atom in **2**, **4**, **5**, and **6** is clearly smaller. Atomic charges of H200 and H300 are exactly equal in complex **2**, reflecting that the $C_s$ symmetry of this complex is not only geometrical but topological as well. On the other hand, these charges are clearly different in complex **1**, while notably they are equal (within two significant digits)

in the similar octahedral Mn complex **3**. It is also interesting to note that atomic charges of H200 and H300 are clearly more negative in the borane adduct H$^{i}$Pr$_2$bzamBH$_3$ (last row in Table 4) than in any of the six complexes, while H100 charges are very similar (even identical in the case of complex **2**), as expected.

**Table 4**
QTAIM (ZORA-B1PW91/QZ4P) atomic charges, *Q* (e), for selected atoms of complexes **1** and **2**, and of borane adduct, compared to complexes **3** and **4** [13b], and to **5** and **6** [13a].

| *Complex* | *M*[a] | *H100* | *H200* | *H300* | *B1* | *N1* | *N2* |
|---|---|---|---|---|---|---|---|
| **1** | 1.043 | –0.592 | –0.496 | –0.482 | 1.843 | –1.401 | –1.135 |
| **2** | 0.628 | –0.621 | –0.439 | –0.439 | 1.764 | –1.377 | –1.050 |
| **3** | 1.056 | –0.586 | –0.504 | –0.500 | 1.823 | –1.436 | –1.173 |
| **4** | 0.603 | –0.587 | –0.514 | –0.491 | 1.787 | –1.404 | –1.121 |
| **5** | 0.603 | –0.595 | –0.514 | –0.512 | 1.778 | –1.372 | –1.125 |
| **6** | 0.605 | –0.591 | –0.458 | –0.467 | 1.750 | –1.394 | –1.128 |
| **B**[b] | ----- | –0.621 | –0.601 | –0.602 | 1.794 | –1.306 | –1.112 |

[a]M = Mn1 (**1** and **3**), Ru1 (**2** and **4**), Rh1 (**5**), Ir1 (**6**). [b]B = borane adduct H$^{i}$Pr$_2$bzamBH$_3$.

There are several local topological properties of the electron density (i.e., calculated at a *bcp*) that have been successfully used to analyze the bonding in compounds containing transition metals. The electron density ($\rho_b$), the ellipticity ($\varepsilon_b$), the Laplacian of the electron density ($\nabla^2\rho_b$), the kinetic energy density ratio ($G_b/\rho_b$) and the total energy density ratio ($H_b/\rho_b$, with $H_b(r) = G_b(r) + V_b(r)$ and $\frac{1}{4}\nabla^2\rho_b(r) = 2G_b(r) + V_b(r)$, where $V_b(r)$ is the potential energy density) are by far the most common [1–4]. Values of these topological properties for selected bonds of complexes **1** and **2** are collected in Table 5, which shows that bond path lengths (*bpl*'s) of M–H and B–H bonds are clearly longer in both compounds than the corresponding interatomic distances (Tables 1 and 2) due to their curvature. For instance, Ru1–H200 and Ru1–H300 *bpl*'s are both 0.052 Å longer than their corresponding interatomic distances, while Mn1–H200 and Mn1–H300 *bpl*'s are, respectively, 0.095 Å and 0.125 Å longer, showing a symmetric curvature in complex **2** but asymmetric in complex **1**. In fact, all topological parameters for Ru1-H200 and Ru1-H300 are nearly identical (Table 5), as well as those for B1-H200 and B1-H300 in complex **2**, while this is not the case for the equivalent values in complex **1**, where significant differences are found. For instance, while the ellipticity of Ru1-H200 and Ru1-H300 bonds is, respectively, 1.14 and 1.13, values for Mn1-H200 and Mn1-H300 are, respectively, 1.06 and 1.25. Even greater differences are found in other local magnitudes, like the Laplacian of the electron density (compare 6.63 e Å$^{-5}$ for both Ru1–H bonds in **2** with 6.00 e Å$^{-5}$ and 5.32 e Å$^{-5}$ in **1** for, respectively, Mn1–H200 and Mn1–H300).

The different nature of the interactions involving H-bridging atoms in **1** and **2** can be appreciated by comparing, for instance, the local topological properties of the B1–H200 and B1–H300 bonds with those of the B1–H100 bond in the same complexes and with the three B–H bonds in the borane adduct $H^iPr_2bzamBH_3$, since the latter is a good reference for borane compounds without attached transition-metal atoms, where the $BH_3$ moiety has three topologically equivalent B-H bonds. The large values of the electron density ($\rho_b > 1$), the large and negative values of the Laplacian ($\nabla^2\rho_b << 0$), the large and negative values of the total energy density ratio ($H_b/\rho_b < -1$), the small values of the ellipticity, and the straight bond paths for the latter are typical of well known open-shell bonds with cylindrical symmetry between light atoms (covalent σ bonds in MO terminology). On the contrary, values for B1–H200 and B1–H300 bonds in **1** and **2**, in particular their curvature and the higher values for the ellipticity, are characteristic of multicenter interactions (see below for a more detailed description involving also the metal atoms) [3].

On the other hand, it is well known that integral topological properties (i.e., calculated over a whole atomic basin, over an interatomic surface or along a bond path) are even more useful than local topological properties for characterizing bonds in transition-metal compounds [1–4]. The delocalization index, δ(A–B), which estimates the number of electron pairs delocalized between atoms A and B, is by far the integral topological property that has been most frequently used in QTAIM studies. In the last column of Table 5, values for the delocalization index of selected bonds for **1** and **2** are included. As expected from our previous discussion, there is a clear asymmetry in the values for δ(M–H) (0.448 and 0.430 for H200 and H300, respectively) and δ(B–H) (0.364 and 0.374 for H200 and H300, respectively) in complex **1**, while for complex **2** there is a complete symmetry in this index too.

**Table 5**

Topological parameters (ZORA-B1PW91/QZ4P) of selected bonds of complexes **1** and **2**, and of borane adduct.

| Bond[a] | Complex[b] | $d$ (Å)[c] | $\rho_b$ (e Å$^{-3}$)[d] | $\nabla^2\rho_b$ (e Å$^{-5}$)[e] | $H_b/\rho_b$ (h e$^{-1}$)[f] | $G_b/\rho_b$ (h e$^{-1}$)[g] | $\varepsilon_b$[h] | $\delta$(A–B)[i] |
|---|---|---|---|---|---|---|---|---|
| M–H200 | **1** | 1.773 | 0.589 | 5.997 | –0.312 | 1.025 | 1.065 | 0.449 |
| | **2** | 1.801 | 0.656 | 6.634 | –0.340 | 1.048 | 1.136 | 0.575 |

| | | | | | | | | |
|---|---|---|---|---|---|---|---|---|
| M–H300 | **1** | 1.830 | 0.571 | 5.320 | –0.315 | 0.967 | 1.253 | 0.431 |
| | **2** | 1.801 | 0.656 | 6.627 | –0.340 | 1.047 | 1.130 | 0.575 |
| B1–H100 | **1** | 1.195 | 1.229 | –9.115 | –1.120 | 0.601 | 0.009 | 0.550 |
| | **2** | 1.192 | 1.198 | –6.981 | –1.091 | 0.683 | 0.004 | 0.540 |
| | **B** | 1.207 | 1.143 | –6.482 | –1.066 | 0.750 | 0.103 | 0.521 |
| B1–H200 | **1** | 1.338 | 0.875 | –3.301 | –0.909 | 0.645 | 0.271 | 0.364 |
| | **2** | 1.364 | 0.868 | –3.892 | –0.904 | 0.590 | 0.351 | 0.366 |
| | **B** | 1.229 | 1.074 | –5.503 | –1.031 | 0.758 | 0.139 | 0.506 |
| B1–H300 | **1** | 1.329 | 0.888 | –3.495 | –0.920 | 0.644 | 0.256 | 0.374 |
| | **2** | 1.365 | 0.866 | –3.899 | –0.903 | 0.588 | 0.353 | 0.366 |
| | **B** | 1.225 | 1.087 | –5.707 | –1.038 | 0.757 | 0.128 | 0.509 |
| M–N2 | **1** | 2.081 | 0.535 | 8.089 | –0.164 | 1.222 | 0.084 | 0.517 |
| | **2** | 2.152 | 0.584 | 8.902 | –0.197 | 1.264 | 0.175 | 0.641 |
| B1–N1 | **1** | 1.483 | 1.204 | 7.193 | –0.988 | 1.406 | 0.009 | 0.451 |
| | **2** | 1.491 | 1.173 | 8.707 | –0.948 | 1.468 | 0.013 | 0.451 |
| | **B** | 1.580 | 0.894 | 8.197 | –0.804 | 1.536 | 0.015 | 0.375 |
| $M–(CO)_{eq}$[j] | **1** | 1.795 | 1.007 | 14.570 | –0.393 | 1.406 | 0.119 | 1.138 |
| $M–(CO)_{ax}$ | **1** | 1.801 | 1.007 | 14.491 | –0.393 | 1.400 | 0.073 | 1.133 |
| M–C[j] | **2** | 2.160 | 0.635 | 6.016 | –0.323 | 0.988 | 0.839 | 0.539 |

[a]M = Mn1 (**1**), Ru1 (**2**). [b] **B** = borane adduct $H^iPr_2bzamBH_3$. [c]Bond path length. [d]Electron density at the *bcp*. [e]Laplacian of the electron density at the *bcp*. [f]Total energy density ratio at the *bcp*. [g]Kinetic energy density ratio at the *bcp*. [h]Ellipticity at the *bcp*. [i]Delocalization index. [j]Average values.

Delocalization indexes of the non-bonding M···B1, M···N1, and M···H100 interactions in complexes **1** and **2** (Table 6) also contribute to shed some light on the characteristics of these interactions. Although δ(M···N1) and δ(M···H100) are indeed very small (they are included in the table only for comparison purposes), δ(M···B1) values are not negligible at all but comparable in magnitude to, or even greater than, values found in many M–M interactions. For instance, δ(M–M) values for $[M_2(CO)_{10}]$ (M = Mn, Tc, Re) complexes, where a *bp* between metal atoms exists, are 0.281, 0.336, and 0.246, respectively, whereas δ(M···M) values for the H-bridged intermetallic interactions of $[M_3(\mu\text{-}H)_3(CO)_{12}]$, in which there is no *bp* between metal atoms, are 0.129, 0.134, and 0.134, respectively [3s]. Analogously, in complex $[Ru_3(\mu\text{-}H)_2(\mu_3\text{-}MeImCH)(CO)_9]$ ($Me_2Im$ = 1,3-dimethylimidazol-2-ylidene), δ(Ru–Ru) is 0.458 for the metal-metal interaction where a *bp* does exist,

while δ(Ru···Ru) is 0.246 and 0.169 for the two H-bridged interactions where no *bp* exists [3j]. In fact, by adding up δ(M–H200) and δ(B1–H200) values for the bonding interactions, with one half the value of δ(M···B1) for the non-bonding M···B1 interaction in each M(μ-H)$_2$B ring, a total of 0.896 (**1**) and 1.065 (**2**) electron pairs are obtained, which is approximately the same as if one single M–B1 bond, without the bridging hydrogen, was present in each cluster. Similarly, by adding up δ(M–H300) and δ(B1–H300) values with the other half of the δ(M···B1) value a total of 0.888 (**1**) and 1.065 (**2**) electron pairs are obtained. For a comparison, in the previously studied borane complexes **3**–**6**, values between 0.9 and 1.1 are found for these additions [13]. In other words:

$$\delta(M-H200)+\delta(B1-H200)+\frac{1}{2}\delta(M\cdots B1)\approx 1$$

$$\delta(M-H300)+\delta(B1-H300)+\frac{1}{2}\delta(M\cdots B1)\approx 1$$

which clearly represents two 3c-2e bonding interactions in the M(μ-H)$_2$B moiety of each complex.

**Table 6**

Delocalization indexes, δ(A···B), for selected non-bonding A···B interactions of **1** and **2** (ZORA-B1PW91/QZ4P level).

| Complex[a] | M···B1 | M···N1 | M···H100 |
|---|---|---|---|
| **1** | 0.166 | 0.074 | 0.033 |
| **2** | 0.248 | 0.094 | 0.050 |

[a]M = Mn1 (**1**), Ru1 (**2**).

The integrated electron density over the whole interatomic surface, $\int_{A\cap B}\rho$, which is also an integral property, is an additional tool for characterizing bonding interactions since it is related to the bond strength [1–4]. Table 7, which collects this magnitude for several bonding interactions in **1** and **2**, shows that M–H200 and M–H300 bonds are slightly weaker than the B1-H200 and B1-H300 bonds, while the B1–H100 bonds are clearly stronger than the former, with values similar to the ones found in the borane adduct (last row in Table 7), which are typical of fully localized covalent bonds (note also the differences in delocalization indexes between both kinds of B–H bonds in the last column of Table 5). Nevertheless, the values found for M–H200 and M–H300 are comparable to those obtained, for

instance, for the Zn–Zn bond of $[Zn_2(\eta^5\text{-}C_5Me_5)_2]$ (1.252 e $Å^{-1}$) [3e] or even for the Mo–Mo of $[Mo_2(\mu\text{-}Ac)_2(\mu\text{-}Cl)_2Cl_4]^{2-}$ (1.083 e $Å^{-1}$), which has a formal bond order of three [3p], showing that they are not particularly weak. Additionally, as clearly seen in Table 7, the asymmetry in complex 1 between Mn1-H200-B1 and Mn1-H300-B1 interactions is once again noteworthy, while for complex 2 both interactions are completely symmetrical.

**Table 7**

Integrated electron density over the whole interatomic surface, $\int_{A\cap B}\rho$ (e $Å^{-1}$), for selected bonding interactions of **1**, **2**, and the borane adduct (ZORA-B1PW91/QZ4P level).

| Complex[a] | M–H200 | M–H300 | B1–H100 | B1–H200 | B1–H300 | M–N2 |
|---|---|---|---|---|---|---|
| **1** | 1.220 | 1.140 | 1.941 | 1.491 | 1.466 | 1.306 |
| **2** | 1.347 | 1.347 | 1.968 | 1.500 | 1.500 | 1.557 |
| **B**[b] | ----- | ----- | 1.793 | 1.898 | 1.891 | ----- |

[a]M = Mn1 (**1**), Ru1 (**2**). [b]**B** = borane adduct $H^iPr_2bzamBH_3$.

Further insight into the multicenter character of the bonding in complexes **1** and **2** may be obtained from the Electron Localization Function (ELF) [29]. ELF of complexes **1** and **2** is depicted in Figure 4, where two trisynaptic valence basins V(M,H,B) located on the H200 and H300 atoms are shown for each complex, as previously observed for $B_2H_6$ and $Al_2H_4(CH_3)_2$, for instance, where two V(B,H,B) and V(Al,C,Al) basins, respectively, are present [30]. They can be easily distinguished in Figure 4 from more typical disynaptic valence basins, like V(M,C) or V(C,O), corresponding to M–CO bonds, and from monosynaptic basins, likes those located at carbonyl O atoms, V(O), corresponding to lone pairs.

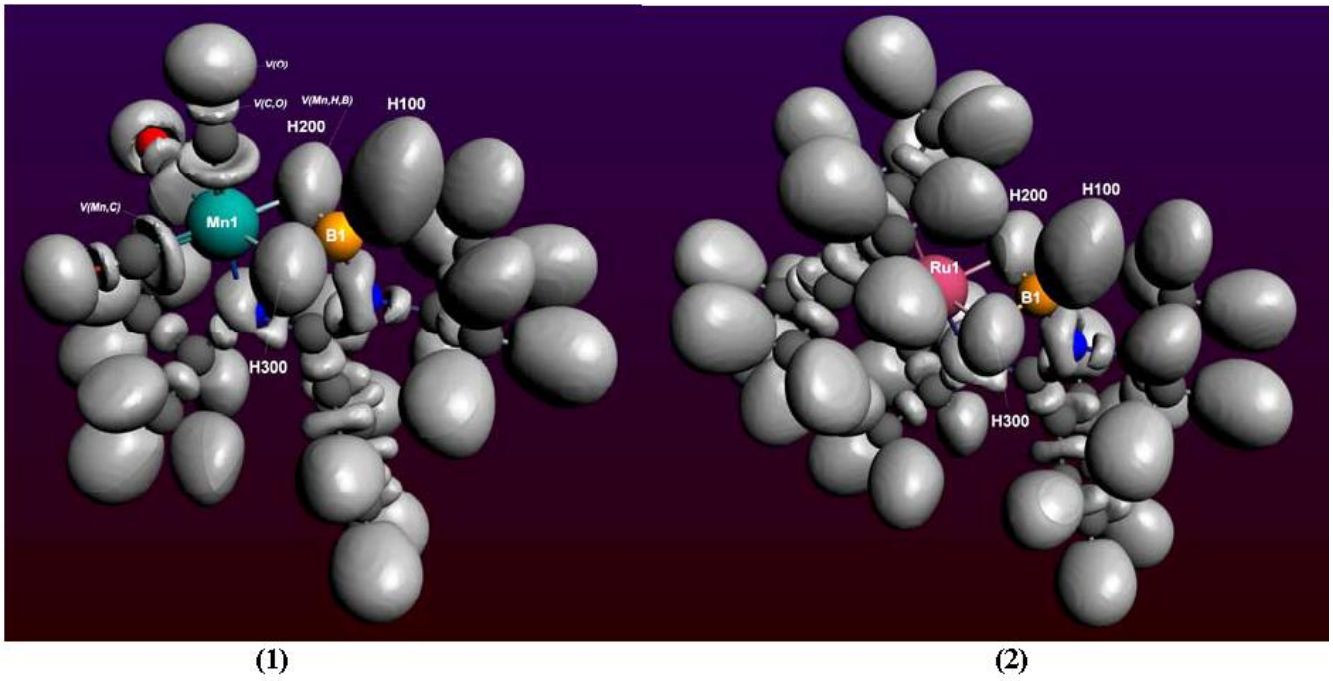


**Fig. 4** Electron Localization Function (ELF) isosurface (ZORA-B1PW91/QZ4P level), at η = 0.8 e Å$^{-3}$, for complexes **1** and **2**. Additional and larger images are included in the Supplementary Material file.

Figure 5 is a representation of the Laplacian of the electron density in the H200–M–H300 plane of both complexes, which is also very useful to analyze M–H and M–CO interactions, among others. This figure shows that the valence shell of each M atom has a nearly perfect cubic shape due to its octahedral coordination. Valence shell charge concentrations (VSCC's) of H atoms are distorted toward the midpoint of each M's valence shell edge, where it is located its valence shell charge depletion (VSCD), showing clearly the curvature of each M–H interaction. This behavior, typical of multicenter bonds, has been previously observed in many other H-bridged systems, like in the previously mentioned Mn, Ru, Rh, and Ir borane complexes [13], and also in metal cluster complexes, such as $[M_3(\mu\text{-}H)_3(CO)_{12}]$ (M = Mn, Tc, Re) [3s], $[Ru_3(\mu\text{-}H)_2(\mu^3\text{-}MeImCH)(CO)_9]$ [3j,3r], $[Os_3(\mu\text{-}H)_2(CO)_{10}]$ [3n], $[Os_3(\mu\text{-}H)(\mu\text{-}OH)(CO)_{10}]$ [3n] and $[Os_3(\mu\text{-}H)(\mu\text{-}Cl)(CO)_{10}]$ [3n], among others, some of them studied from both theoretical and experimental electron densities. On the other hand, the key-lock mechanism prototypical of the Dewar-Chatt-Duncanson (DCD) donor-acceptor model for interactions between a transition-metal atom and a non-metal atom is clearly appreciated here in Mn1–CO bonds. Each C atom points its VSCC directly toward a VSCD of the metal atom along a straight line, with no curvature at all in this case.

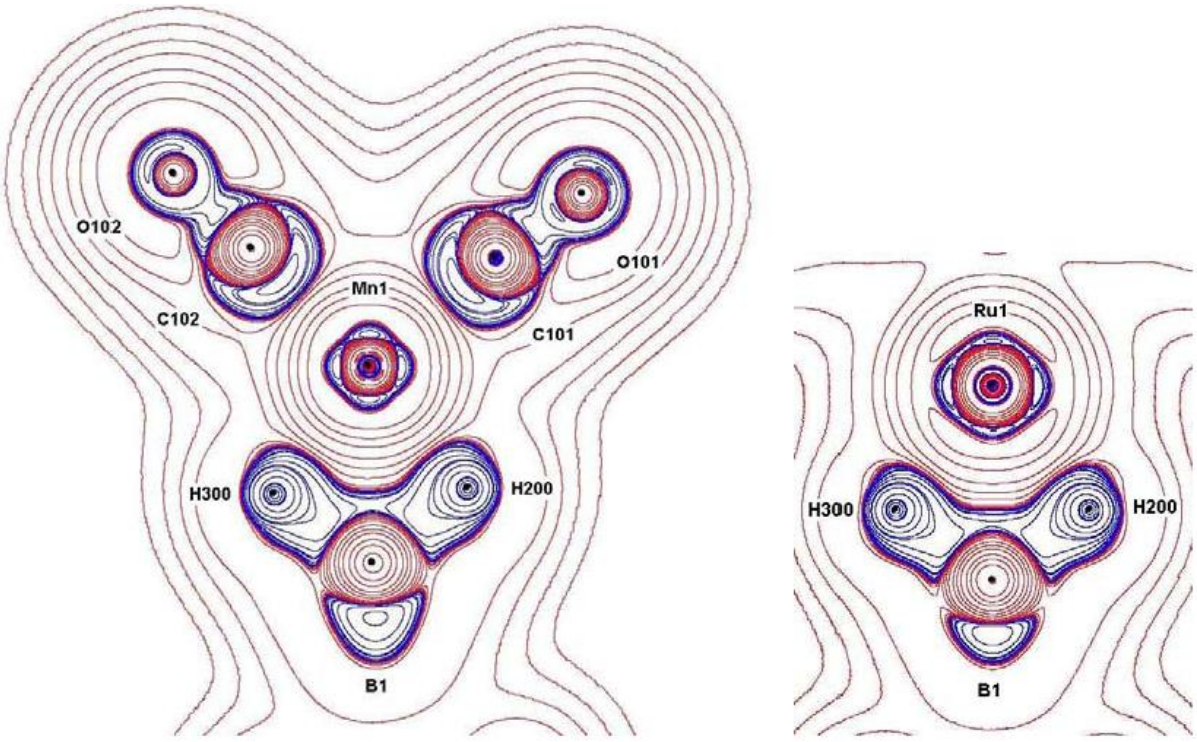


(1) (2)

**Fig. 5** Laplacian of the electron density in relevant planes (B3P86/6-311++G(2df,2pd)/WTBS(Ru) level) containing the metal atoms of complexes **1** and **2** (contour levels at 0.0 and ± (1,2,4,8) × $10^n$ e $Å^{-5}$, with n ranging from +3 to –3). Blue and red lines represent negative and positive values, respectively. Larger images are included in the Supplementary Material file.

## 4. Conclusions

Several local and integral topological properties of the electron density associated to the different interatomic interactions present in the transition-metal borane complexes [Mn($\kappa^3$*N,H,H*-$^i$Pr$_2$bzamBH$_3$)(CO)$_3$] (**1**) and [Ru($\eta^5$-C$_5$Me$_5$)($\kappa^3$*N,H,H*-$^i$Pr$_2$bzamBH$_3$)] (**2**) (H$^i$Pr$_2$bzamBH$_3$ = N-trihydridoborane-N,N'-bis(isopropyl)benzamidinate) have been obtained using non-relativistic and relativistic QTAIM calculations. A comparative analysis of these results has allowed the establishment of the following main conclusions:

(*a*) Most M–L interactions (L = CO, $^i$Pr$_2$bzam) in both complexes follow the classical Dewar-Chatt-Duncanson (DCD) donor-acceptor model, as revealed by the key-lock mechanism showed in Laplacian representations as well as by the straight bond paths obtained, among other features. They can be considered classical polar covalent bonds.

(*b*) No M–B bond paths have been obtained for any of the two complexes, although non-negligible delocalization indexes have been calculated for these interactions.

(*c*) All M–H interactions with the $BH_2$ group in both complexes show bond paths that are strongly inwardly curved, with greater curvature near hydrogen atoms than near metal centers. These bonds can be considered intermediate between those of the Shimoi or σ-terminal type ($\kappa^1$*H* coordination of the B–H bond, no M–B interaction) and those of the agostic type ($\kappa^2$*B,H* coordination of the B–H bond, M–B and M–H interactions).

(*d*) The two M–H interactions in the Ru complex **2** are equivalent to each other, as well as the two B–H interactions within the Ru(μ-H)$_2$B moiety. On the contrary, Mn–H interactions in complex **1** are not completely equivalent, one of them being more agostic than the other, i.e. Mn1–H300 (more curved and higher ellipticity).

(*e*) Two 3c-2e bonding interactions may be postulated for the M(μ-H)$_2$B moiety in both complexes.

(*f*) A comparison of the results described in this work with those previously reported for σ-borane complexes (M = Mn (**3**), Ru (**4**), Rh (**5**), and Ir (**6**)), containing a similar tripod $\kappa^3$*N,H,H* borane ligand but different additional ligands, shows that the bonding similarities and differences within each particular M(μ-H)$_2$B moiety are not related to the type of metal atom, nor even to its coordination geometry, but mainly to the molecular symmetry, since a plane of symmetry that contains atoms M, B, H100, N1 and N2 is present in complexes with equivalent interactions (**2** and **3**) but it is absent in those with non-equivalent interactions (**1**, **4**, **5**, and **6**).

**Acknowledgements**

This work has been supported by Spanish MINECO projects (MAT2016-78155-C2-1-R and CTQ2016-75218-P) and Principality of Asturias grants (GRUPIN14-060 and GRUPIN14-009).

**Supplementary material**

CCDC1921463, CCDC1921464, and CCDC1921465 contain the supplementary crystallographic data for this paper. These data can be obtained free of charge via https://www.ccdc.cam.ac.uk/structures/. Selected X-ray diffraction data, atomic coordinates for the theoretically optimized geometries and additional figures are available at https://doi.org/10.1016/j.molstruc.20xx.xx.xxx. Checkpoint files of geometry optimizations and electronic structure calculations for the borane adduct, and for complexes **1** and **2** are available from the authors upon request.

## References


[1] (a) R.F.W. Bader, Atoms in Molecules: A Quantum Theory, Clarendon Press, Oxford, UK, 1990;
(b) P. Coppens, X-Ray Charge Densities and Chemical Bonding, International Union of Crystallography and Oxford University Press, Oxford, UK, 1997;
(c) P.L.A. Popelier, Atoms in Molecules: An Introduction, Prentice Hall, Harlow, UK, 2000;
(d) C.F. Matta, R.J. Boyd (Eds.), The Quantum Theory of Atoms in Molecules, Wiley-VCH, Weinheim, Germany, 2007;
(e) C. Gatti, P. Macchi (Eds.), Modern Charge Density Analysis, Springer, Heidelberg, Germany, 2012;
(f) D. Stalke (Ed.), Electron Density and Chemical Bonding (2 vols.), Springer, Heildelberg, Germany, 2012;
(g) G. Frenking, S. Shaik (Eds.), The Chemical Bond, Wiley-VCH, Weinheim, Germany, 2014.

[2] (a) T.S. Koritsanszky, P. Coppens, Chem. Rev. 101 (2001) 1583–1627;
(b) F. Cortés-Guzmán, R.F.W. Bader, Coord. Chem. Rev. 249 (2005) 633–662;
(c) C. Gatti, Z. Kristallogr. 220 (2005) 399–457;
(d) P. Coppens, B.B. Iversen, F.K. Larsen, Coord. Chem. Rev. 249 (2005) 179–195;
(e) P. Macchi, Angew. Chem. Int. Ed. 48 (2009) 5793–5795;
(f) Y. Ling, Y. Zhang, Ann. Rep. Comput. Chem. 6 (2010) 65–77;
(g) P. Macchi, Crystallogr. Rev. 19 (2013) 58–101;
(h) M.R.V. Jørgensen, V.R. Hathwar, N. Bindzus, N. Wahlberg, Y.S. Chen, J. Overgaard, B.B. Iversen, IUCr J. 1 (2014) 267–280;
(i) A. Nassour, S. Domagala, B. Guillot, T. Leduc, C. Lecomte, C. Jelsch, Acta Crystallogr. B 73 (2017) 610–625.

[3] (a) P. Macchi, D.M. Proserpio, A. Sironi, J. Am. Chem. Soc. 120 (1998) 13429–13435;
(b) P. Macchi, L. Garlaschelli, A. Sironi, J. Am. Chem. Soc. 124 (2002) 14173–14184;
(c) P. Macchi, A. Sironi, Coord. Chem. Rev. 238 (2003) 383–412;
(d) L.J. Farrugia, C. Evans, M. Tegel, J. Phys. Chem. A 110 (2006) 7952–7961;
(e) J.F. Van der Maelen, E. Gutiérrez-Puebla, A. Monge, S. García-Granda, I. Resa, E. Carmona, M.T. Fernández-Díaz, G.J. McIntyre, P. Pattison, H.P. Weber, Acta Crystallogr. B 63 (2007) 862–868;
(f) A. Reisinger, N. Trapp, I. Krossing, S. Altmannshofer, V. Herz, M. Presnitz, W. Scherer, Angew. Chem. Int. Ed. 46 (2007) 8295–8298;

(g) C. Gatti, D. Lasi, Faraday Discuss. 135 (2007) 55–78;

(h) J. Overgaard, H.F. Clausen, J.A. Platts, B.B. Iversen, J. Am. Chem. Soc. 130 (2008) 3834–3843;

(i) D. Himmel, N. Trapp, I. Krossing, S. Altmannshofer, V. Herz, G. Eickerling, W. Scherer, Angew. Chem. Int. Ed. 47 (2008) 7798–7801;

(j) J.A. Cabeza, J.F. Van der Maelen, S. García-Granda, Organometallics 28 (2009) 3666–3672;

(k) L.J. Farrugia, C. Evans, D. Lentz, M. Roemer, J. Am. Chem. Soc. 131 (2009) 1251–1268;

(l) K. Götz, M. Kaupp, H. Braunschweig, D. Stalke, Chem. Eur. J. 15 (2009) 623–632;

(m) L.J. Farrugia, P. Macchi, Struct. Bonding 146 (2010) 127–158;

(n) J.F. Van der Maelen, S. García-Granda, J.A. Cabeza, Comput. Theor. Chem. 968 (2011) 55–63;

(o) C. Gatti, Struct. Bonding 147 (2012) 193–286;

(p) J.F. Van der Maelen, J.A. Cabeza, Inorg Chem. 51 (2012) 7384–7391;

(q) J.A. Cabeza, J.M. Fernández-Colinas, P. García-Álvarez, E. Pérez-Carreño, V. Pruneda, J.F. Van der Maelen, Chem. Eur. J. 19 (2013) 9251−9260;

(r) J.F. Van der Maelen, S. García-Granda, AIP Conf. Proc. 1642 (2015) 563–566;

(s) J.F. Van der Maelen, J.A. Cabeza, Theor. Chem. Acc. 135 (2016) 64;

(t) J. Ruiz, D. Sol, L. García, M.A. Mateo, M. Vivanco, J.F. Van der Maelen, Organometallics 38 (2019) 916–925.

[4] (a) P. Macchi, J.-M. Gillet, F. Taulelle, J. Campo, N. Claisere, C. Lecomte, IUCr J. 2 (2015) 441–451;

(b) A. Genoni, L. Bučinský, N. Claiser, J. Contreras-García, B. Dittrich, P.M. Dominiak, E. Espinosa, C. Gatti, P. Giannozzi, J.-M. Gillet, D. Jayatilaka, P. Macchi, A.Ø. Madsen, L. Massa, C.F. Matta, K.M. Merz Jr., P.N.H. Nakashima, H. Ott, U. Ryde, K. Schwarz, M. Sierka, S. Grabowsky, Chem. Eur. J. 24 (2018) 10881−10905.

[5] (a) A. Staubitz, A.P.M Robertson, I. Manners, Chem. Rev. 110 (2010) 4079−4124;

(b) C.W. Hamilton, R.T. Baker, A. Staubitz, I. Manners, Chem. Soc. Rev. 38 (2009) 279−293;

(c) T.B. Marder, Angew. Chem. Int. Ed. 46 (2007) 8116−8118;

(d) F.H. Stephens, V. Pons, R.T. Baker, Dalton Trans. (2007) 2613−2626.

[6] (a) E.M. Leitao, T. Jurca, I. Manners, Nat. Chem. 5 (2013) 817−829;

(b) T.J. Clark, K. Lee, I. Manners, Chem. Eur. J. 12 (2006) 8634−8648;

(c) H.C. Johnson, T.N. Hooper, A.S. Weller, Top. Organomet. Chem. 49 (2015) 153−220.

[7] H.C. Johnson, T.N. Hooper, A.S. Weller, in: E. Fernández, A. Whiting (Eds.), Synthesis and Application of Organoboron Compounds, Springer Int. Publ., New York, 2015, pp. 153−220.

[8] (a) A.M. Lunsford, J.H. Blank, S. Moncho, S.C. Haas, S. Muhammad, E.N. Brothers, M.Y. Darensbourg, A.A. Bengali, Inorg. Chem. 55 (2016) 964−973;
(b) A.E. Nako, A.J.P. White, M.R. Crimmin, Dalton Trans. 44 (2015) 12530−12534;
(c) R. Dallanegra, A.B. Chaplin, A.S. Weller, Angew. Chem. Int. Ed. 48 (2009) 6875−6878.

[9] (a) J.R. Vance, A. Schäfer, A.P.M. Robertson, K. Lee, J. Turner, G.R. Whittell, I. Manners, J. Am. Chem. Soc. 136 (2014) 3048−3064;
(b) A.N. Marziale, A. Friedrich, I. Klopsch, M. Drees, V.R. Celinski, J. Schmedt auf der Günne, S.J. Schneider, J. Am. Chem. Soc.135 (2013) 13342−13355;
(c) A.B. Chaplin, A.S. Weller, Inorg. Chem. 49 (2010) 1111−1121;
(d) C.J. Stevens, R. Dallanegra, A.B. Chaplin, A.S. Weller, S.A. Macgregor, B. Ward, D. McKay, G. Alcaraz, S. Sabo-Etienne, Chem. Eur. J. 17 (2011) 3011−3020;
(e) L.J. Sewell, G.C. Lloyd-Jones, A.S. Weller, J. Am. Chem. Soc. 134 (2012) 3598−3610;
(f) H.C. Johnson, E.M. Leitao, G.R. Whittell, I. Manners, G.C. Lloyd-Jones, A.S. Weller, J. Am. Chem. Soc. 136 (2014) 9078−9093.

[10] (a) D.J. Wolstenholme, K.T. Traboulsee, A. Decken, G.S. McGrady, Organometallics 29 (2010) 5769−5772;
(b) G. Alcaraz, A.B. Chaplin, C.J. Stevens, E. Clot, L. Vendier, A.S. Weller, S. Sabo-Etienne, Organometallics 29 (2010) 5591−5595;
(c) D. Vidovic, D.A. Addy, T. Kräm̈er, J. McGrady, S.J. Aldridge, J. Am. Chem. Soc. 133 (2011) 8494−8497;
(d) M.W. Drover, E.G. Bowes, L.L Schafer, J.A. Love, A.S. Weller, Chem. Eur. J. 22 (2016) 6793−6797;
(e) H.C. Johnson, A.P.M. Robertson, A.B. Chaplin, L.J. Sewell, A.L. Thompson, M.F. Haddow, I. Manners, A.S. Weller, J. Am. Chem. Soc. 133 (2011) 11076−11079.

[11] (a) M. Shimoi, S.I. Nagai, M. Ichikawa, Y. Kawano, K. Katoh, M. Uruichi, H. Ogino, J. Am. Chem. Soc. 121 (1999) 11704−11712;
(b) G.J. Kubas, Metal Dihydrogen and σ-Bond Complexes, Springer, New York, 2001;
(c) G. Alcaraz, S. Sabo-Etienne, Angew. Chem. Int. Ed. 49 (2010) 7170−7179.

[12] (a) D. Sharmila, B. Mondal, R. Ramalakshmi, S. Kundu, B. Varghese, S. Ghosh, Chem. Eur. J. 21 (2015) 5074–5083;

(b) C. Lenczyk, D.K. Roy, B. Ghosh, J. Schwarzmann, A.K. Phukan, H. Braunschweig, Chem. Eur. J. 25 (2019) 8585-8589.

[13] (a) J. Brugos, J.A. Cabeza, P. García-Álvarez, A.R. Kennedy, E. Pérez-Carreño, J. F. Van der Maelen, Inorg. Chem. 55 (2016) 8905–8912;

(b) J. Brugos, J.A. Cabeza, P. García-Álvarez, E. Pérez-Carreño, J. F. Van der Maelen, Dalton Trans. 46 (2017) 4009–4017.

[14] N. Oshima, H. Suzuki, Y. Moro-Oka, Chem. Lett., 13 (1984) 1161-1164.

[15] (a) CrysAlisPro RED, version 1.171.37.35, Oxford Diffraction Ltd., Oxford, UK, 2014 (for compound $H^iPr_2bzamBH_3 \cdot 0.5(C_7H_8)$);

(b) CrysAlisPro RED, version 1.171.36.28, Oxford Diffraction Ltd., Oxford, UK, 2013 (for compound **1**);

(c) CrysAlisPro RED, version 1.171.38.43, Oxford Diffraction Ltd., Oxford, UK, 2015 (for compound **2**).

[16] A. Altomare, M. C. Burla, M. Camalli, G. L. Cascarano, C. Giacovazzo, A. Guagliardi, A. G. C. Moliterni, G. Polidori, R. Spagna, J. Appl. Crystallogr., 32 (1999) 115-119.

[17] G. M. Sheldrick, Acta Cryst. A, 64 (2008) 112-122.

[18] L. J. Farrugia, J. Appl. Crystallogr., 45 (2012) 849-854.

[19] MERCURY, CSD 3.8 (build RC2), Cambridge Crystallographic Data Centre, Cambridge, UK, 2016.

[20] (a) G. Eickerling, R. Mastalerz, V. Herz, W. Scherer, H.J. Himmel, M. Reiher, J. Chem. Theory Comput. 3 (2007) 2182–2197;

(b) G. Eickerling, M. Reiher, J. Chem. Theory Comput. 4 (2008) 286–296;

(c) N. Hebben, H.J. Himmel, G. Eickerling, C. Hermann, M. Reiher, V. Herz, M. Presnitz, W. Scherer, Chem. Eur. J. 13 (2007) 10078–10087;

(d) M. Reiher, A. Wolf, Relativistic Quantum Chemistry: The Fundamental Theory of Molecular Science, Wiley-VCH, Weinheim, Germany, 2009.

[21] M.J. Frisch, et al., GAUSSIAN09, Revision B.01, Gaussian Inc, Wallingford, Connecticut, 2010.

[22] (a) C. Lee, W. Yang, R.G. Parr, Phys. Rev. B 37 (1988) 785–789;

(b) J.P. Perdew, Phys. Rev. B 33 (1986) 8822–8824;

(c) A.D. Becke, J. Chem. Phys. 98 (1993) 5648–5652.

[23] (a) S. Huzinaga, B. Miguel, Chem. Phys. Lett. 175 (1990) 289–291;

(b) S. Huzinaga, M. Klobukowski, Chem. Phys. Lett. 212 (1993) 260–264.

[24] E. van Lenthe, E.J. Baerends, J. Comput. Chem. 24 (2003) 1142–1156.

[25] E.J. Baerends, et al., ADF2012, Revision 01d, SCM, Theoretical Chemistry, Vrije Universiteit, Amsterdam, The Netherlands, 2012.

[26] T.A. Keith, AIMAll, Version 15.09.27, TK Gristmill Software, Overland Park, Kansas, 2015.

[27] F. Biegler-König, J. Schönbohm, J. Comput. Chem. 23 (2002) 1489–1494.

[28] M. Kohout, DGrid 4.6, Max Planck Institute for Physical Chemistry of Solids, Dresden, Germany, 2011.

[29] (a) E. Matito, M. Solá, Coord. Chem. Rev. 253 (2009) 647–665;
(b) F. Feixas, E. Matito, M. Duran, J. Poater, M. Solà, Theor. Chem. Acc. 128 (2011) 419–431;
(c) M. Kohout, F.R. Wagner, Y. Grin, Theor. Chem. Acc. 108 (2002), 150–156.

[30] (a) Y. Grin, A. Savin, B. Silvi, in: G. Frenking, S. Shaik (Eds.), The Chemical Bond: Fundamental Aspects of Chemical Bonding, Wiley-VCH, Weinheim, Germany, 2014, pp. 345–382;
(b) B. Silvi, R. J. Gillespie, in: C. F. Matta, R. J. Boyd (Eds.), The Quantum Theory of Atoms in Molecules: From Solid State to DNA and Drug Design, Wiley-VCH, Weinheim, Germany, 2007, pp. 141–162.